IEEE Robotics and Automation Letters (RAL) paper presented at the
2020 IEEE/RSJ International Conference on Intelligent Robots and Systems (IROS)
October 25-29, 2020, Las Vegas, NV, USA (Virtual)

Detection and Control of Air Liquid Interface With an Open-Channel Microfluidic Chip for Circulating Tumor Cells Isolation From Human Whole Blood

Bilal Turan, Yusuke Tomori, Taisuke Masuda, *Member, IEEE*, Ruixuan Weng, Larina Tzu-Wei Shen, Satoshi Matsusaka, and Fumihito Arai, *Member, IEEE*

***Abstract*— We have proposed a bio-automation system to isolate and recover circulating tumor cells (CTCs) individually from whole blood. An open-channel microfluidic chip-based approach is used to isolate the CTCs. The proposed microfluidic chip design can form a stable air-liquid interface. CTCs are trapped by the gaps in between the pillars of the microfluidic chip due to capillary force associated with the meniscus of the air-liquid interface. We propose a chip design to stabilize air-liquid interface and sample flow speed. We introduce an image analysis algorithm to detect the position of the air-liquid interface. Using the visual feedback from the image analysis algorithm, a control system is proposed to control air-liquid interface position. We succeeded in stabilizing the flow speed, making it feasible for the isolation of 5 mL of whole blood to be completed within 30 min. We achieved an average of position error of air-liquid interface of 4 µm with standard deviation of 7 µm. We have confirmed that air-liquid interface position is a deciding factor for trapping area of CTCs. By controlling air-liquid interface position, we have achieved trapping CTCs in a narrow band with a high concentration.**

I. Introduction

Isolation of rare cells such as circulating tumor cells (CTCs) has a wide range of applications [1]. Several studies have analyzed the genetic mutations carried by CTCs, comparing the mutations to those of primary tumors or correlating the findings to the severity or spread of the patient's disease [2-4]. A challenge for CTC researchers is the difficulty of collecting CTCs at the single-cell level. In the recent years, the importance of single-cell analysis has grown rapidly for various fields, including drug discovery and regenerative medicine [5,6]. Due to the inhomogeneous states in a cellular cluster, the analysis results suggest only average states. In contrast, some of mechanisms cannot be explained by average states because it depends on a threshold factor or stochastic component [7-9]. The determination of the true mechanism requires analysis of the cluster at the single-cell level to avoid the loss of information associated with ensemble averaging [10, 11].

Numerous studies proposed to isolate CTCs from blood using biological and physical properties. Epithelial cell adhesion molecule (EpCAM) is mainly employed as an isolation method utilizing biological properties but is known for having low trap rate [12]. On the other isolation methods using physical properties to trap CTCs such as filtration-based devices suffer from clogging [13]. To overcome issues such as low trap rate and clogging, we have pioneered a bio-automation system utilizing an open-channel microfluidic chip-based approach to isolate CTCs and CTC clusters from whole blood samples [14]. Open-channel microfluidic chip simplifies recovering CTCs from the microfluidic chip surface after isolation. Blood sample is introduced between a supply unit and the open-channel microfluidic chip and held there. A pressure gradient is generated and can be controlled by introducing more blood sample with a syringe pump. Cells within the blood sample, including CTCs, are then trapped in the gaps in between the pillars of the microfluidic chip due to capillary force associated with the meniscus of the air-liquid interface [15]. After the isolation, the trapped CTCs can be detected using fluorescence microscopy and machine learning methods, then recovered using a micro-pipette. Our proposed system aims to automate isolation, detection and recovery of the rare cells such as CTCs from whole blood sample.

Proposed method simplifies recovery of CTCs after isolation and minimizes probable damage to CTCs that could be caused by flow pressure. However, an open-channel microfluidic chip introduces new challenges. One such challenge is to stabilize the flow speed of the blood sample. Previously we succeeded the isolation of CTCs from 5 ml of whole blood which took between 30 min to 60 min [14]. As the condition of the blood sample deteriorates over time it is important to finish isolation within a determined amount of time. To achieve stable sample flow microfluidic chip design is crucial as well as precise control of the syringe pumps. If too much blood sample is introduced at a time, the microfluidic chip might overflow. Similarly, if the flow speed of the blood sample through microfluidic chip is less than the speed of the syringe pump for the waste, then air will be sucked inside the syringe with the blood sample. This in turn decreases the accuracy of the flow control. Therefore, another challenge is minimizing the air introduced to the waste syringe.

This work was supported in part by START Program from Japan Science and Technology Agency, JST., and supported in part by AMED under Grant Number JP19he2202003.

B. Turan, Y. Tomori, T. Masuda, R. Weng and F. Arai are with the Department of Micro-Nano Mechanical Science & Engineering, Nagoya University, Furo-cho, Chikusa-ku, Nagoya, Japan, 464-8603 (e-mail: bilal@biorobotics.mech.nagoya-u.ac.jp).

[2]L. T. Shen and S. Matsusaka are with the Department of Clinical Research and Regional Innovation, Faculty of Medicine, University of Tsukuba, 1-1-1 Tennodai, Tsukuba, Japan, 305-8577

Copyright ©2020 IEEE

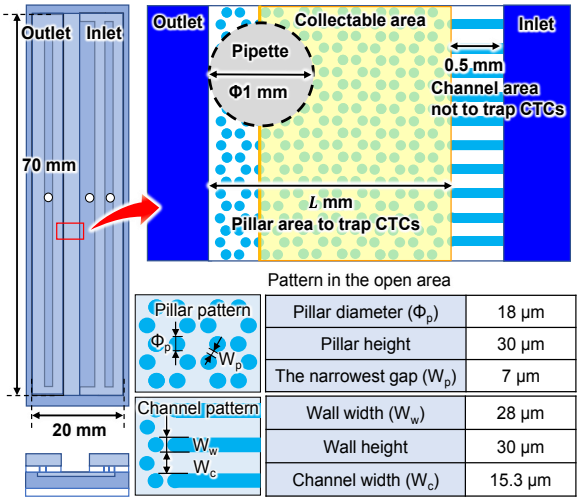

Figure 1. Dimensions of the microfludic chip and the design parameters of the micro-pillar array and channels.

Stabilizing air-liquid interface in an open-channel microfluidic chip is yet another challenge. Due to the small amount of blood sample, evaporation plays a major role. The inertia of the system makes the control of the air-liquid interface very challenging. The stable formation and positioning of the meniscus of the air-liquid interface is crucial for the trap rate of CTCs. Therefore, meniscus of the air-liquid interface needs to be detected and its position should be accurately controlled. To address these challenges, we describe an open-channel microfluidic chip design to minimize the air introduced, as well as an automation system to detect and control the position of the meniscus of the air-liquid interface using this microfluidic chip.

II. Materials and Methods

A. *Microfluidic-chip Design in Consideration of Air-Liquid Interface*

By controlling the air-liquid interface position precisely, we can control the area on the microfluidic chip that CTCs are most likely to be trapped. Using an open-channel microfluidic chip we aim to trap rare cells such as CTCs from whole blood sample. Using an open-channel microfluidic chip enables easy access and trapped rare cells can be isolated with the help of a micro-pipette.

The design of the microfluidic chip is as Fig. 1 shows the blood sample is introduced into a liquid reservoir and an air-liquid interface is formed. The blood which flows through the microfluidic chip by the help of gravity and capillary forces is collected through the outlet. Generally, CTCs are 15±10 μm in diameter [16], whereas red blood cells and white blood cells are 6 to 8 and 10 to 12 μm in diameter, respectively [17]. We designed the microfluidic chip based on this information to isolate CTCs according to size. Micropillars are arranged in a honeycomb pattern across the microfluidic chip surface, forming a pocket for trapping CTCs. The most important dimension is the distance between two micropillars (W_p)

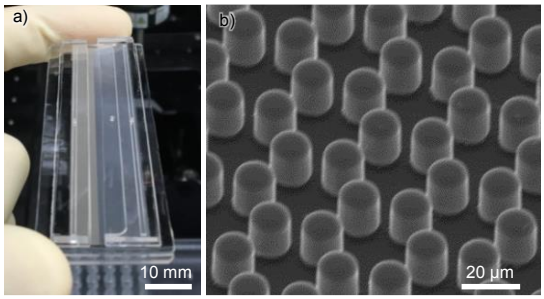

Figure 2. (a) Fabricated open-channel microfluidic channel. (b) The fabricated micropillars.

within a regular hexagon as this distance determines the rates of both trapping CTCs and removing blood cells. From the preliminary experiment, 7 μm was found to be the most efficient W_p, and 18 μm was chosen as the diameter of the micropillars [14]. The height of the fluid channel was 30 μm across the entire microfluidic chip. A channel area is introduced in order to avoid trapping CTCs outside of the collectable area with wall width of 28 μm and channel width of 15.3 μm. Fig. 2 illustrates the fabricated microfluidic chip.

Stability of the blood sample flow within the open-channel microfluidic chip depends on the velocity of the capillary flow V_{cap} at the outlet. V_{cap} is described as the following formula:

$$V_{cap} = \frac{\gamma}{6\mu} \cdot \frac{h \cdot f}{L}$$

where γ is the surface tension of the sample, μ is the viscosity of the sample, h is the height of pillar pattern, f is the non-dimensional number described with the aspect ratio of pillar pattern and the contact angle of the sample on the substrate, and L is the distance from the meniscus to the outlet. The parameters γ, μ, h and f are assumed to be constant, therefore we define the constant C as the following:

$$C = \sqrt{\frac{\gamma}{3\mu}} \cdot \sqrt{h \cdot f}$$

then we can re-write the formula for V_{cap} as:

$$V_{cap} = \frac{C^2}{2L}$$

The state of the flow on the chip depends on the relation between the suction velocity in the outlet V_{out} and V_{cap}. As Fig. 3(a) illustrates when $V_{out} > V_{cap}$, the flow is split, and the state is intermittent flow causing air to be sucked inside the waste syringe pump. In contrast, when $V_{out} \leq V_{cap}$, the state is continuous flow since capillary flow prevents splitting of the flow and leads to less air suction as Fig 3(b) illustrates.

We designed the chip length accordingly, to reduce the air suction. The upper limit of the distance from the meniscus of the air-liquid interface to the outlet, L was derived from the condition $V_{out} \leq V_{cap}$. The maximum throughput under under this condition is described as the following formula using the cross-section area into the outlet, S_{outlet}:

$$q_{max} = S_{outlet} \cdot V_{cap}$$

then V_{cap} and the maximum throughput under the condition $V_{out} \leq V_{cap}$ depend on the parameter L, which results in the following formula:

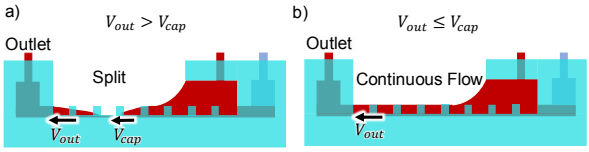

Figure 3.(a) Capillary flow speed is not enough and flow is interrupted, air is introduced to waste syringe. (b) Capillary flow speed is sufficient, continuous flow is achieved.

$$q_{max} = S_{outlet} \cdot \frac{C^2}{2}$$

In order to find L, we first find the constant C. The optimal chip length is found experimentally. The microfluidic chip is fabricated according to experimental findings.

B. *Detection and Control of Air-Liquid Interface*

Fig. 4(a) shows a microscopy image of the air-liquid interface. The right side of the image shows the blood sample reservoir which is darker, and the pillars are less distinct due to blood covering them. The left side has a higher intensity as the blood cells are traveling in between the pillars. We can define the position of the air-liquid interface as the boundary between where the blood cells move above the pillars and flow in between them. But because the exact position is difficult to determine; a steep decrease in average intensity can be used as a heuristic for the air-liquid interface position, as the side of the air liquid interface with blood sample reservoir is darker.

We calculate the average intensity of each column through the image's x-axis. A gaussian filter is applied to remove the noise as plotted in Fig. 4(b). Then the derivative of the smoothed average intensity is calculated as Fig. 4(c) shows. The peak of this derivative function is illustrated with a circle. The peak of the derivative where a steep decrease in average intensity occurs is chosen as detected air-liquid interface position. We have confirmed that peak of the derivative as a heuristic can be used for the air-liquid interface control.

In order to use the air-liquid interface heuristic, we need to ascertain whether air-liquid interface exists within the image or not. The honeycomb like pattern of the micropillar design is utilized to ascertain whether air-liquid interface exist within image or not. Due to the honeycomb like pattern of micropillars, the average intensity of columns fluctuates as Fig. 4(b) shows. This fluctuation is more pronounced at the left side of the image where the pillars are more distinct compared to the pillars within the blood sample reservoir. Taking the smoothed average intensity as a baseline and subtracting it from the average intensity of the columns makes this fluctuation easily visible as Fig. 5(a) shows. Moving variance of the average intensity of the columns is calculated as Fig. 5(b) shows. Using this moving variance, we decide whether air-liquid interface exists within the image or not. When air-liquid interface is not formed there are two cases to consider. The first case being before the air-liquid interface is formed when there is not enough blood sample in the reservoir. The second case is if the entire visible area is filled with blood sample due to reservoir overflow of the sample.

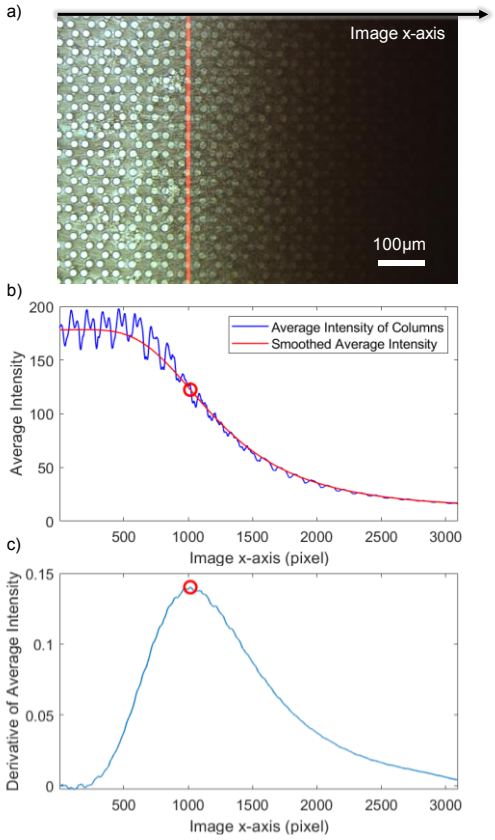

Figure 4. (a) Air-liquid interface, and its detected position, (b) average intensity of each column and smoothed average intensity (c) derivative of the smoothed average intensity, peak is the detected air-liquid interface position.

We calculate $\bar{x}_{start}$ as the average of the first 128 pixels of moving variance. Similarly, $\bar{x}_{end}$ is calculated as the average of the last 128 pixels. Lastly $\bar{x}_{all}$ is calculated as the average of the entire moving variance. When air-liquid interface is formed in the image the ratio of $\bar{x}_{start}$ is significantly larger to $\bar{x}_{end}$ and their ratio is used to determine the existence of the air-liquid interface. In the absence of the sample, all pillars are visible, resulting in a large $\bar{x}_{all}$. When the chip is overflown with sample, no pillars are visible, resulting in a small $\bar{x}_{all}$. In both cases the ratio of $\bar{x}_{start}$ and $\bar{x}_{end}$ is small. The following formula is used to determine all three cases:

$$\frac{\bar{x}_{start}}{\bar{x}_{end}} > 50, \qquad Air\ Liquid\ Int.exist$$

$$\frac{\bar{x}_{start}}{\bar{x}_{end}} < 50\ \&\ \bar{x}_{all} > 10, \qquad No\ Sample$$

$$\frac{\bar{x}_{start}}{\bar{x}_{end}} < 50\ \&\ \bar{x}_{all} < 10, \qquad Overshoot$$

In case of *Air Liquid Int. exist* the air-liquid interface is in the image and its value is determined by the peak value of the derivative. In the case of *No Sample* the air-liquid interface position is fixed as 3096, and in the case of *Overshoot*, the air-liquid interface position is fixed as 0. The result of the detection is then used as visual feedback for the controller.

Control of the air-liquid interface position is achieved by setting the flow speed of sample introduction and waste suction. From the start of the sample introduction until the

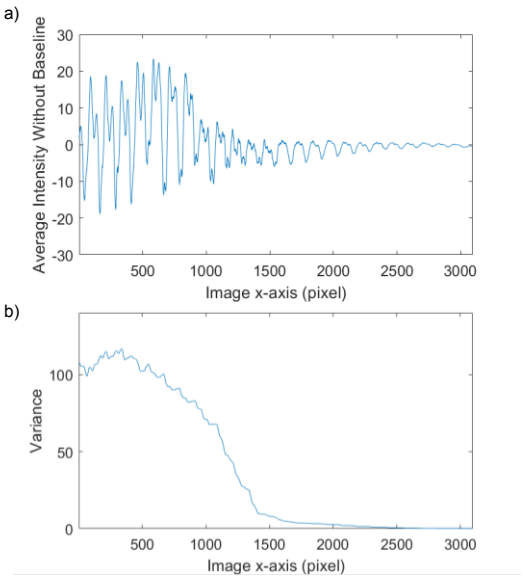

Figure 5. (a) Fluctuation of average intensity due to visibility of pillar pattern, (b) moving variance of the average intensity.

time air-liquid interface is formed within the image, flow velocities are set to a constant value. Once the air-liquid interface reaches the target position, then the flow speeds for supply and suction are actively controlled. Fig. 6 illustrates the flow chart of the air-liquid interface controller. A simple P-controller is used for supply and suction. The outputs of these controllers are subtracted or added to an initial supply and suction speed. Initial supply and suction speed are the set flow speeds when air-liquid interface position is at target value. Throughout the isolation, two syringe pumps only work in one direction. This is a design decision to not re-introduce waste back into the chip, and to not suck the sample back once it is introduced to the chip. Hence if the final output is below zero, we stop supply and suction pumps respectively.

Fig. 7 shows the components of the system. All components can be controlled through a personal computer. Four syringe pumps are connected to the microfluidic chip which controls sheath liquid flow, blood sample supply, waste suction and micro pipetting sheath flow. A camera connected to a microscope is used for visual feedback for air-liquid interface control during CTC isolation. Microfluidic chip is mounted on an XY-linear stage for easier access to any point in the microfluidic chip. A micropipette attached to a XYZ-linear stage is used to collect the isolated CTCs from the chip.

III. RESULTS

A. Velocity of Capillary Flow and Optimal Chip Length

The optimal length of the microfluidic chip is determined experimentally with the goal to achieve isolation of CTCs from 5 mL of whole blood in 30 mins. Fig. 8(a) illustrates the experimental setup. An open microfluidic chip with the same pillar pattern as proposed microfluidic chip is prepared with the parameters as in Fig. 8(a). The blood sample is prepared with the same conditions when isolating CTCs. Introducing a drop of blood to the chip, the time and penetration distance l is recorded.

The constant C can be described as the following formula and was derived from the results of recording time and the penetration distance l of sample on the chip which is shown in Fig. 8(b).

$$C = \frac{l}{\sqrt{t}}$$

The minimum C was calculated as 4.1 $mm/\sqrt{s}$. For the continuous flow condition, the upper limit of the distance from the meniscus of the air-liquid interface to the outlet, the limit of L was calculated as 1.7 mm.

B. Position Control of Air-Liquid Interface

Whole blood sample is diluted with the same volume of PBS (EDTA-2Na solution) to avoid clogging. We spiked green fluorescent protein (GFP)-expressing human gastric cancer cells (GCIY-EGFPs) into the sample as CTC surrogates. A total volume of 10 mL is then introduced into the microfluidic chip.

The supply speed is set at a constant speed of 5.6 µm/s to finish the isolation in 30 min. Until the air-liquid interface is formed within the image the suction is set to 2.8 µm/s to remove excess sheath. Air-liquid interface control starts after the air-liquid interface reached the target position. Fig. 9 shows the position error of the detected air-liquid interface.

Until the air-liquid interface is formed 3 min passed, after that air-liquid interface is controlled during the isolation of the CTCs which is finished within 30 min (video attachment). Through the isolation air-liquid interface stays within the image and only recedes just before isolation ends, as there is no more blood sample to keep the air-liquid interface at the target position. Therefore, we exclude the last 2 min of the experiment. The average position error of air-liquid interface was 4 µm with a standard deviation of 7 µm.

C. Controlling the Trapping Area for CTCs using Air-Liquid Interface Control

The position of air-liquid interface within the microfluidic chip can be controlled, and the trapping area for CTCs are decided by the accuracy of the air-liquid interface control. As illustrated in Fig. 10 the proposed air-liquid interface detection algorithm and the trapping area overlap. In Fig 10. (b) the red line indicates the detected air-liquid interface position, and the CTCs are trapped around the air-liquid interface position.

To assess the trapping area of the CTCs we conducted an experiment with the proposed control algorithm. For comparison, another experiment was conducted where flow speeds of the syringe pumps are manually controlled by a user. Following CTC isolation, using sheath liquid the microfluidic chip is cleaned, and remaining red blood cells are washed away. Then staining is performed, and lastly the chip is cleaned with sheath liquid. The surface area of the microfluidic chip is scanned, and microscopic images of CTCs trapped by the micropillars are acquired and merged. Fig. 11 demonstrates part of the microfluidic chip after isolation, for both cases. Trap position is defined with inlet as zero position, and by

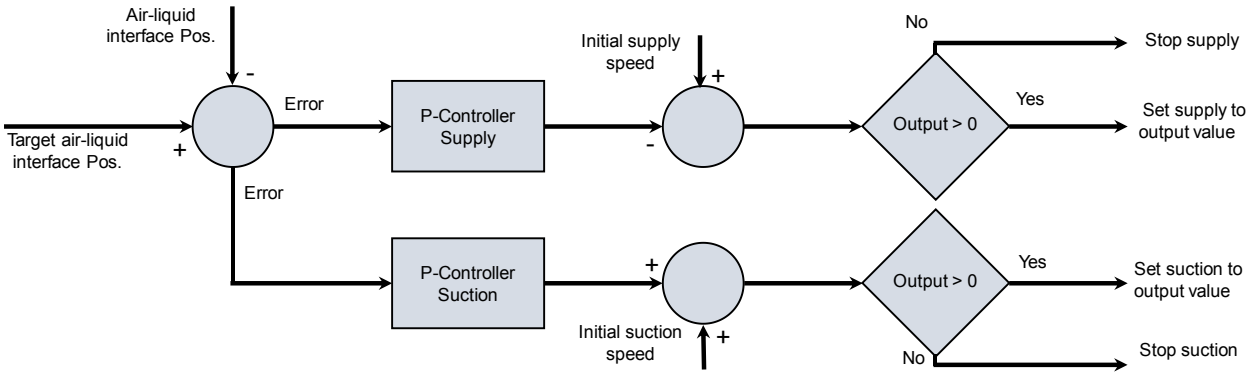

Figure 6. Controller design for supply and suction pumps.

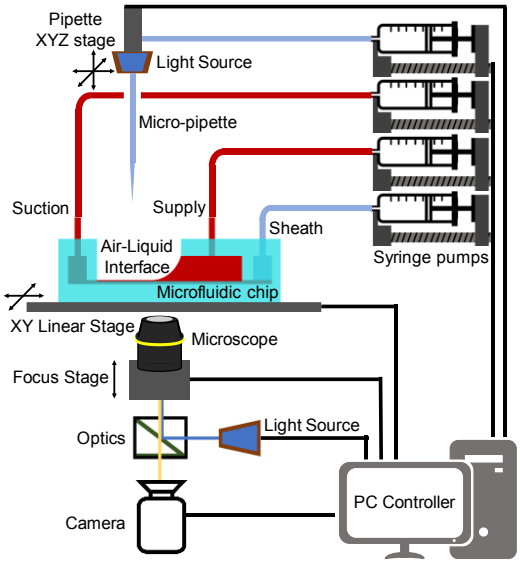

Figure 7. Components of the system.

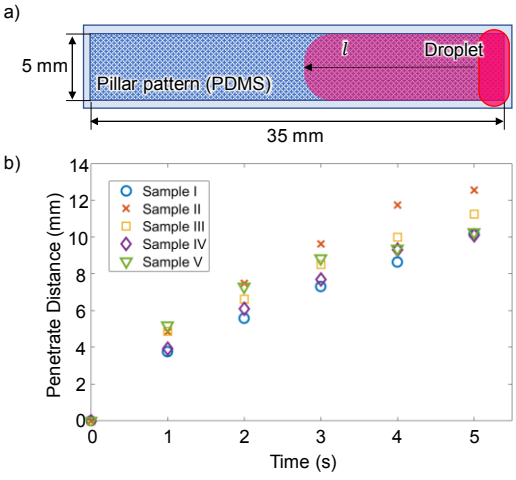

Figure 8. (a) Experimental setup to find optimal chip length, (b) Penetrate distances of the droplets of blood samples in time.

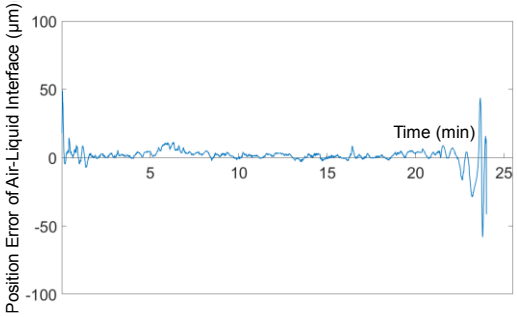

Figure 9. Position error of air-liquid interface position throughout isolation.

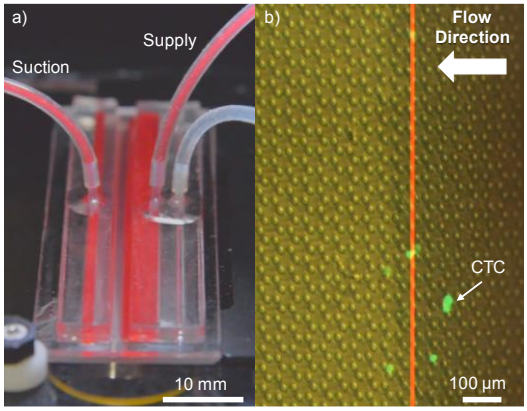

Figure 10. (a) The experimental setup, the air-liquid interface is formed at the liquid reservoir. (b) CTCs are trapped at the detected air-liquid interface.

dividing the distance between inlet and outlet into equal sections trap probabilities are calculated as the total area of CTCs in that section. As Fig. 11(b) shows, it is possible to have a concentrated trapping area for CTCs, by controlling air-liquid interface position in comparison to manual control as in Fig. 11(a). From the trap probabilities calculated we confirmed 85% of the trapped CTCs are within the collectable area.

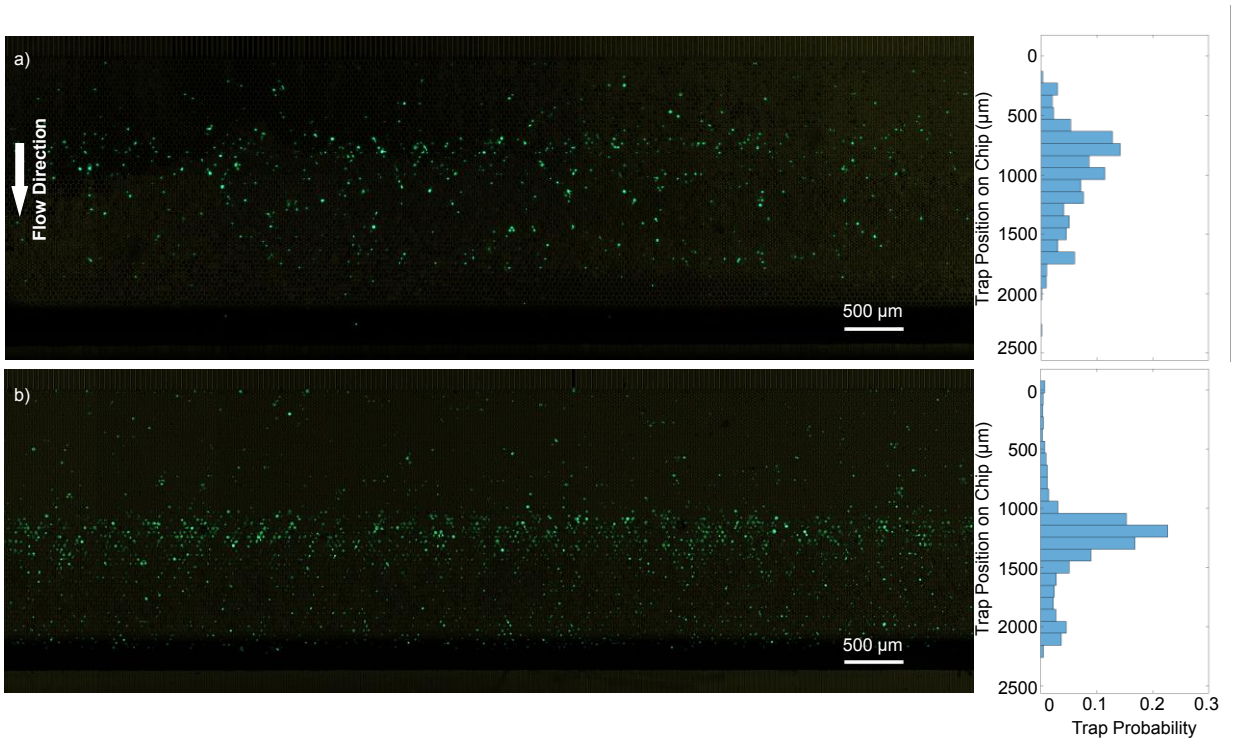

Figure 11. (a) Air-liquid interface is controlled manually and as a result the trapping area of CTCs are wide. (b) When the air-liquid interface is controlled by the proposed control system, the CTCs are trapped within a narrow band. Green cells are CTC.

IV. Discussion

Flow control within an open-channel microfluidic chip has many challenges compared to a closed-channel chip. The flow velocity of the sample is limited by the capillary forces and chip design. The possibility of air being sucked into the waste syringe coupled with external factors such as evaporation renders the formation of a robust control system challenging.

The proposed chip design and controller decreases the air sucked to sub-mL (data not shown), increasing the accuracy of the air-liquid interface position control. The isolation of blood sample finished in 30 min whereas in previous work the isolation time was uncertain (30-60 min) [14]. However, this decrease in isolation time results in the reduction of the collectable area for CTCs. The collectable area is 1.7 mm wide considering physical constraints from the micro-pipette and it is feasible to isolate the CTCs in collectable area when an accuracy of 4 µm is achieved in air-liquid interface control. From Fig. 11(b), CTCs are trapped in the collectable area with a probability of 85%, and only 15% of CTCs pass through the gaps. Further optimizing the micro-pillar design is required to increase the trapping rate of CTCs in the collectable area. Our open-channel microfluidic chip causes less damage during all processes, including isolation and recovery [14].

Automation of CTC isolation with the proposed method is possible. The trapped CTCs can be detected using machine learning algorithms [18], which enable automation of recovery of CTCs individually via micro-pipette.

V. Conclusion

We have proposed a bio-automation system utilizing an open-channel microfluidic chip-based approach to isolate and recover CTCs individually from whole blood samples. We designed an open-channel microfluidic chip, and by controlling the air-liquid interface within the chip, isolation of 5 mL of whole human blood was achieved in 30 min. An average of 4 µm position error of air-liquid interface was attained with standard deviation of 7 µm. It is possible to control the trapping area of CTCs through the position of air-liquid interface. A trapping probability of 85% was achieved within the collectable area.

After the isolation, the CTCs can be observed using fluorescence microscopy, and using a micro-pipette CTCs can be collected with ease from the open-channel chip surface. We have achieved automation in isolation of CTCs which is the most vital part of the proposed bio-automation system. This work explores an uncharted area for rare cell isolation as it can isolate rare cells from whole blood samples containing a large number of cells unlike current cell sorter systems. Regarding future studies, CTC detection and individual recovery can be integrated to achieve complete automation.

In this work CTCs are used for isolation experiments, however proposed bio-automation system can also be applied to the other small samples of cells. Furthermore, this system has some potential to recover rare particles from miscellaneous, such as undifferentiated stem cells contained

in transplanted cells, and fetal erythroblasts contained in the blood of pregnant mothers.

REFERENCES

[1] Nagrath, Sunitha, et al. "Isolation of rare circulating tumour cells in cancer patients by microchip technology." *Nature* 450.7173 (2007): 1235.

[2] Maheswaran, Shyamala, et al. "Detection of mutations in EGFR in circulating lung-cancer cells." *New England Journal of Medicine* 359.4 (2008): 366-377.

[3] Miyamoto, David T., et al. "Androgen receptor signaling in circulating tumor cells as a marker of hormonally responsive prostate cancer." *Cancer discovery* 2.11 (2012): 995-1003.

[4] Sabine, Riethdorf et al., "Clinical applications of the CellSearch platform in cancer patients". Advanced Drug Delivery Reviwes. 125 (2018): 102–121.

[5] Cantor, Charles R. "Biotechnology in the 21st century." *Trends in biotechnology* 18.1 (2000): 6-7.

[6] Cohen, Joel I. "Harnessing biotechnology for the poor: challenges ahead for capacity, safety and public investment." *Journal of Human Development* 2.2 (2001): 239-263.

[7] Carlo, Dino Di, and Luke P. Lee. "Dynamic single-cell analysis for quantitative biology." (2006): 7918-7925.

[8] Lidstrom, Mary E., and Michael C. Konopka. "The role of physiological heterogeneity in microbial population behavior." *Nature chemical biology* 6.10 (2010): 705.

[9] Wang, Daojing, and Steven Bodovitz. "Single cell analysis: the new frontier in 'omics'." *Trends in biotechnology* 28.6 (2010): 281-290.

[10] Tsutsuyama, Masayuki, et al, "Detection of circulating tumor cells in drainage venous blood from colorectal cancer patients using a new filtration and cytology-based automated platform" *PloS one* 14.2 (2019): e0212221.

[11] Kondo, Yuurin, et al., "KRAS mutation analysis of single circulating tumor cells from patients with metastatic colorectal cancer". 17.1 (2017):311.

[12] Gabriel, Marta Tellez, et al. "Circulating tumor cells: a review of non–EpCAM-based approaches for cell enrichment and isolation." Clinical chemistry 62.4 (2016): 571-581.

[13] Yusa, Akiko, et al. "Development of a new rapid isolation device for circulating tumor cells (CTCs) using 3D palladium filter and its application for genetic analysis." PloS one 9.2 (2014).

[14] Masuda, Taisuke, et al. "Rare cell isolation and recovery on open-channel microfluidic chip." *PloS one* 12.4 (2017): e0174937.

[15] Inglis, David W., et al. "Continuous microfluidic immunomagnetic cell separation." *Applied Physics Letters* 85.21 (2004): 5093-5095.

[16] Sarioglu, A. Fatih, et al. "A microfluidic device for label-free, physical capture of circulating tumor cell clusters." *Nature methods* 12.7 (2015): 685.

[17] Ji, Hong Miao, et al. "Silicon-based microfilters for whole blood cell separation." *Biomedical microdevices* 10.2 (2008): 251-257.

[18] Turan, Bilal, et al. "High accuracy detection for T-cells and B-cells using deep convolutional neural networks." Robomech J 5,29 (2018).